

Solid-State NMR Study on the Structure and Dynamics of Graphite Electrodes in Sodium-Ion Batteries with Solvent Co-Intercalation

Ines Escher,^[a] Annica I. Freytag,^[b] Juan Miguel López del Amo,^{*[c]} and Philipp Adelhelm^{*[a, b]}

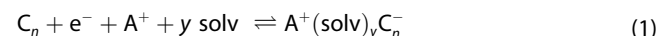
The possibility to co-intercalate sodium ions together with various glymes in graphite enables its use as a negative electrode material in sodium-ion batteries (SIBs). However, the storage mechanism and local interactions appearing during this reaction still needs further clarification. ^1H , ^{13}C and ^{23}Na *ex situ* solid-state NMR (ss-NMR) experiments are performed to obtain insights into the storage mechanism depending on the state of charge (SOC) and the electrolyte solvent used. Distinct differences could be seen depending on the SOC, indicating a

possible change of the solvation shell, differences in the mobility as well as a phase transition at the voltage plateau. Furthermore, exchange experiments reveal information on the sodium ion transport process in the graphitic lattice. The inferior cycling performance of triglyme (3G) (compared to diglyme (2G) and pentaglyme (5G)) is also reflected in the ss-NMR spectra, showing a reduced mobility and stronger interactions between sodium ions, 3G and graphite already at room temperature (RT).

Introduction

Graphite is the most common material used as a negative electrode in lithium-ion batteries (LIBs), showing a capacity of 372 mAh g $^{-1}$.^[1] When moving forward to sodium-ion batteries (SIBs), which are promising alternatives due to more abundant materials and lower cost,^[2] graphite cannot be used with the same electrolyte as in LIBs.^[3] The formation of a binary graphite intercalation compound (intercalation of the bare sodium ions) is thermodynamically unfavorable^[4] and therefore only capacities of around 5–15 mAh g $^{-1}$ can be obtained.^[3] A way to overcome this issue is the use of ether-based electrolytes, in contrast to carbonate-based electrolytes, which are common in LIBs.^[3] This results in the formation of a ternary graphite intercalation compound (*t*-GIC), a co-intercalation of the sodium ions together with their solvent molecules.^[3a,5] The voltage profile of this co-intercalation reaction shows a

characteristic voltage plateau at around 0.6–0.7 V vs. Na $^+$ /Na when using 2G as electrolyte.^[3a,5,6] Equation (1) shows the reaction taking place during electrochemical cycling.^[3a]



The general occurrence of the co-intercalation reaction has been proven by several techniques like *operando* electrochemical dilatometry,^[6f,i,j,m] X-ray diffraction (XRD),^[3b,6c-e,j,7] high resolution transmission electron microscopy (TEM),^[5] Fourier-transform infrared spectroscopy (FTIR) analysis,^[5,7] visualized height change,^[6a,d] Raman^[6b,7] and ss-NMR.^[8] However, the exact stoichiometry [n and y in Equation (1)] and the mechanism of this co-intercalation are not totally clarified yet.

Controversial results have been found especially regarding to the number of co-intercalated 2G molecules per sodium ion [y in Equation (1)]. Kim et al. measured the weight change in a graphite electrode and found a co-intercalation of one 2G molecule per sodium ion. This observation was further supported by energy-dispersive X-ray spectroscopy.^[6a] Additionally, theoretical investigations calculating the solvation energies, showed that a potential second solvent molecule can be removed more easily from the complex than the first one, supporting the idea of one 2G per sodium ion and a partial de-solvation process prior to co-intercalation.^[9] Jung et al. found that a partial de-solvation of [Na(2G) $_2$] $^+$ prior to the co-intercalation reaction must take place to explain the differences between high C-rate behavior of sodium and lithium co-intercalation.^[10] In contrast to this, Seidl et al. and Jache et al. suggested that two 2G molecules encase one sodium ion due to a preferred coordination number of 4–7 for sodium ions.^[3b,6d] In addition, a preferred coordination in the liquid of [Na(2G) $_2$] $^+$ has been found using neutron total scattering and empirical potential structure refinement.^[11] Furthermore, the number of carbon atoms per sodium ion (n) has been calculated from the

[a] I. Escher, Prof. Dr. P. Adelhelm

Humboldt Universität zu Berlin
Institut für Chemie
Brook-Taylor-Str. 2, 12489 Berlin, Germany
E-mail: philipp.adelhelm@hu-berlin.de

[b] Dr. A. I. Freytag, Prof. Dr. P. Adelhelm
Helmholtz-Zentrum Berlin
Joint research group Operando Battery Analysis
Hahn-Meitner-Platz 1, 14109 Berlin, Germany

[c] Dr. J. M. López del Amo
Center for Cooperative Research on Alternative Energies (CIC energiGUNE)
Basque Research and Technology Alliance (BRTA)
Alava Technology Park
Albert Einstein 48, 01510 Vitoria-Gasteiz, Spain
E-mail: jmlopez@cicenergigune.com

 Supporting information for this article is available on the WWW under <https://doi.org/10.1002/batt.202200421>

 © 2022 The Authors. *Batteries & Supercaps* published by Wiley-VCH GmbH. This is an open access article under the terms of the Creative Commons Attribution License, which permits use, distribution and reproduction in any medium, provided the original work is properly cited.

gained capacities, most commonly resulting in values between 20 and 22 (corresponding to a capacity of 100–110 mAh g⁻¹).^[3,6a,c,g,i,12]

The co-intercalation reaction of sodium ions in graphite occurs by a staging process which has been found by several groups using XRD^[6a,c,d,j,7] and Raman spectroscopy.^[6b,7] Kim et al. investigated this system by using *operando* synchrotron-based XRD and found that the upper voltage region can be correlated to a reaction where a lot of different stages exist (number of stages represents the number of graphene layers between intercalant layers).^[6a] During further co-intercalation, stage 2 is formed at the beginning of the plateau and transformed to stage 1 during the plateau. In the following voltage slope stage 1 is further sodiated and ordering phenomena occur.^[6a] This transition (stage 3-2-1) is also supported by other *ex situ* and *in situ* studies.^[6c,d,j] XRD studies further proved that the size of the solvent molecules does not have a strong influence on the interlayer distance in stage 1,^[3b,6a,j,7] showing that the solvent molecules fold between two graphene layers^[7] or are parallel between them.^[6j] The *in situ* Raman experiments fit well with the results found by XRD, showing a stage >2 before the plateau (indicated by a doublet Raman signal) and a stage ≤2 at the beginning of the plateau (single signal).^[6b] Using electrochemical dilatometry (ECD), the voltage decrease after the plateau was correlated with a pseudocapacitive storage mechanism.^[6f,j]

Although 2G is the most common ether used for the co-intercalation of sodium ions in graphite, monoglyme (1G), 3G, tetraglyme (4G) and 5G have also been used successfully.^[3b,6a,d,e,j,7] Herein 3G shows less capacity and an ill-defined voltage profile,^[3b,6d,e,j] which is due to a geometrically unfavorable coordination. Over-^[3b] and under-^[6d] coordination have been suggested, the latter leading to an increased sodium ion – graphite interaction.^[6d] The number of coordinating solvent molecules was assumed to be 3 for 1G,^[3b] 1–2 for 3G,^[3b] 1 for 4G^[3b] and 1 for 5G^[6e] due to the optimum coordination number of 4–7 for sodium ions in solution.^[3b] In contrast, weight change experiments suggested one 1G, 3G and 4G molecule per sodium ion in the intercalated state (but measurements are challenging).^[6a] In addition, it was found that the co-intercalation of 3G as well as 5G, the latter showing a high viscosity at RT, are kinetically controlled, whereas the co-intercalation of 1G, 2G and 4G is governed by thermodynamics.^[6e] This can be seen by a decreased overpotential between charge and discharge at elevated temperatures and low currents for 3G, whereas no influence can be seen on the overpotential of 1G, 2G and 4G in those cases. With rising temperatures, the reaction with 5G becomes thermodynamically limited, in contrast to when 3G is used for which the reaction remains kinetically limited.^[6e]

To gain a deeper understanding of the storage mechanism in *t*-GICs, solid-state nuclear magnetic resonance (ss-NMR) experiments on the co-intercalated materials were performed. Leifer et al. compared in their study the co-intercalation of sodium and lithium ions with 2G in graphite with ss-NMR. They demonstrated that the [Li(2G)]⁺ complex is more tightly connected to the graphene sheets and has a lower mobility

compared to the [Na(2G)]⁺ complex, which indicates weaker interactions to the graphene layers. Those findings can explain the more favorable formation of *t*-GICs with sodium as compared to lithium.^[8] Here, we apply Magic Angle Spinning (MAS) ss-NMR to study the structure of sodium *t*-GICs with 2G at different SOCs. In addition, other linear ether molecules are investigated, and a comparison to the co-intercalation of lithium ions is given.

Results and Discussion

Structure of sodium *t*-GICs with 2G at different SOC

Ex situ solid-state ¹³C NMR experiments have been conducted on graphite samples at different positions of the voltage profile during (de)sodiation, see Figure 1a) for the voltage curve and the cut-off voltages. Before stopping the (de)sodiation at specific voltages, cells were pre-cycled for one cycle. The graphite electrodes were cycled without conductive additive or binder to avoid any possible interference. After reaching specific SOC values, cells were dismantled under argon atmosphere and the graphite samples were packed into 2.5 mm rotors for *ex situ* ss-NMR measurements. Five different samples were measured by ss-NMR during sodiation (S:2V–S:0.01V), where S:0.01V corresponds to the fully intercalated sample. D:0.7V and D:2V represent the de-sodiation process, with D:2V being the fully de-intercalated sample. 1D ¹³C NMR experiments at different degrees of sodiation reveal two signals at around 71 ppm and 62 ppm in all partially and fully intercalated samples (see Figure 1b). These signals, with an approximate ratio of 2:1 are assigned to the CH₂ and CH₃ carbons of the 2G molecules, respectively. The signals between 122–136 ppm can be assigned to the graphitic carbon (signals for aromatic carbon are usually between 120 and 140 ppm^[13]).

Interestingly, for S:1V, S:0.625V and D:0.7V two signals are visible in the region where sodiated graphitic peaks are expected. The peak at 122–125 ppm agrees with the results reported by Leifer et al., corresponding to a down-field shift of the pristine graphitic peak (around 89 ppm).^[8] This shift to higher ppm values can be explained by the interaction of the sodium ions with the conjugated π-system upon co-intercalation similar to the effect of metal doping as explained by Leifer et al.^[8] However, the peak at even higher shift values (134–136 ppm) at low co-intercalation levels has not been reported thus far. Leifer et al. did not perform experiments at these co-intercalation potentials but they did observe a peak in this region after drying the electrode for several days and explained the down-field shift with a change in either the graphene stacking or a change in the solvation shell of the co-intercalated sodium ions. To rule out the possibility of dried-out samples, the experiments at S:1V and S:0.625V were examined more closely by repeating the ¹³C experiments immediately after cycling and then again after 14 days of drying (rotors were opened up inside the glove box and left to dry). The peak shifts at 134–136 ppm were basically unchanged (Figure S1) whereas the peaks at 122–126 ppm decreased

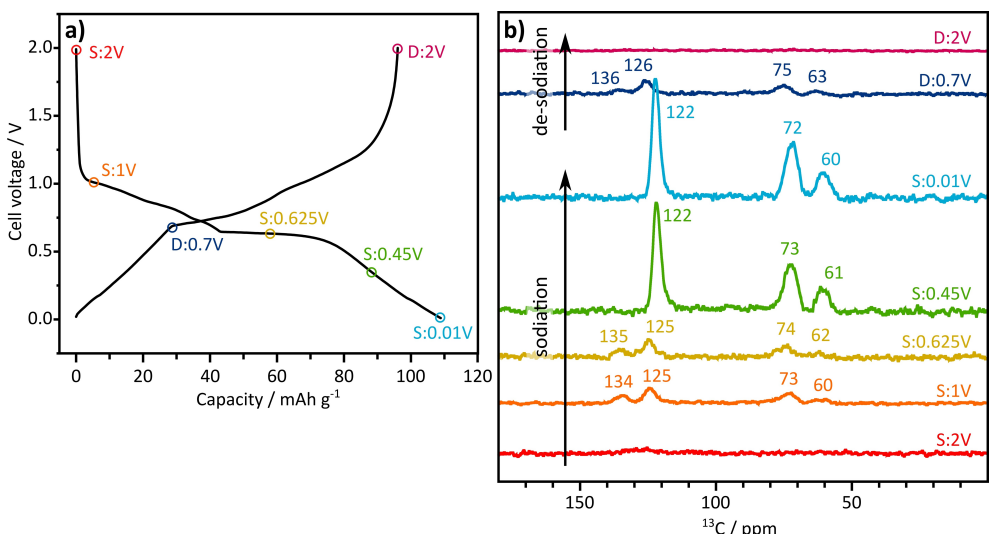


Figure 1. a) Voltage profile of the co-intercalation of sodium ions in graphite (2nd cycle). Specific voltage values during sodiation (S) and de-sodiation (D) are marked at which the measurement is stopped to perform *ex situ* NMR experiments, b) ¹³C MAS NMR spectra of sodium co-intercalated in graphite at different states of charge.

visibly in intensity. This proves that the signal at 135 ppm may also originate from the co-intercalation process and not just from a dried-out sample. This indicates that there is indeed a change in the solvation structure as mentioned by Leifer et al.^[8] However, it is not (only) induced by solvent evaporation but also through partial electrochemical co-intercalation. At low co-intercalation levels the graphene interlayer distance is assumed to be smaller which may favor the coordination of sodium ions with one 2G molecule instead of two. Theoretical calculations showed that sodium ions complexed with only one 2G molecule have a stronger interaction with the graphene layer and are sitting closer to the surface than a complex with two 2G molecules [2.38 Å distance for Na(2G)₁C₂₀ and 5.04 Å for Na(2G)₂C₂₀^[14]]. This results in a stronger direct interaction of the sodium ion with the graphene layers leading to a down-field shift to around 134–136 ppm. However, the peak at 125 ppm indicate that sodium ions are also co-intercalated with two 2G molecules. At higher co-intercalation levels, the graphene interlayer distance might be increased, which makes it more favorable for all the sodium ions to coordinate to two 2G molecules leading to a disappearance of the peak at 134–136 ppm. Further computational studies are necessary to verify the assignment. It has to be kept in mind that also other processes take place between S:1V, S:0.625V and S:0.45V, S:0.01V, that might influence the shift of the ¹³C NMR signal, including a change of the staging^[6a–d],7,15] and probably a change of the stacking order of graphite.^[3b,14,16]

Figure 2 shows the ¹H single pulse NMR spectra of fully co-intercalated graphite samples. During the formation of the t-GICs, sodium ions are co-intercalated into the graphitic lattice together with solvent molecules. In this sense several different ¹H signals are assumed that can be correlated to 2G molecules surrounding sodium ions in the graphitic lattice (see I in Figure 2a) and 2G molecules that are separated from the sodium ions (II). Not all diglyme molecules get intercalated into

the graphitic structure therefore molecules that are adsorbed to the surface are also considered (III). Figure 2b) shows the ¹H single pulse NMR spectra of the fully intercalated t-GIC at RT. Herein, three partially overlapping signals can be seen. Sharp signals at around 3.4 ppm are assigned to free 2G molecules outside of the graphite structure (see III, several small peaks fitted with one peak for simplification), similar to a typical shift of liquid 2G between 3.3 and 3.5 ppm.^[8,13] The low signal width of these molecules indicates a non-restricted mobility that effectively averages out the anisotropic NMR interactions typically present in solid molecules. Two main broad signals are observed in Figure 2b) that are shifted to higher ppm values and are assigned to 2G coordinating sodium ions inside the graphite (6.7 ppm) and non-coordinating 2G inside the graphitic structure (3.8 ppm) (see Figure 2a), I and II). A shift to higher ppm values might be explained by the interaction of the 2G protons with graphite electrons and therefore a deshielding effect by the ring currents of the delocalized π electrons in the graphite and the paramagnetic character of the interaction, which is in agreement with a stronger coordination of the type I 2G with the graphene layers.^[8,17]

Reducing the temperature of the fully intercalated sample to –30 °C (see Figure 2c) results in a broadening of peak I, which is explained by a different mobility of the 2G molecules in the [Na(2G)]⁺ complex at low temperature. In contrast, the signals II and III exhibit a similar line broadening as at RT, indicating that the mobility of the non-coordinating 2G inside the graphitic lattice and the free 2G outside is not dramatically changed at low temperatures. The ratio between glymes coordinating to sodium ions (type I) and the overall amount of glymes as obtained from the signal deconvolution shown in the Figure is similar at RT and –30 °C (59% and 57%, see Supporting Information Table S1), indicating that not the amount of type I glymes is reduced at lower temperatures but only their mobility is restricted. Similar results were found using

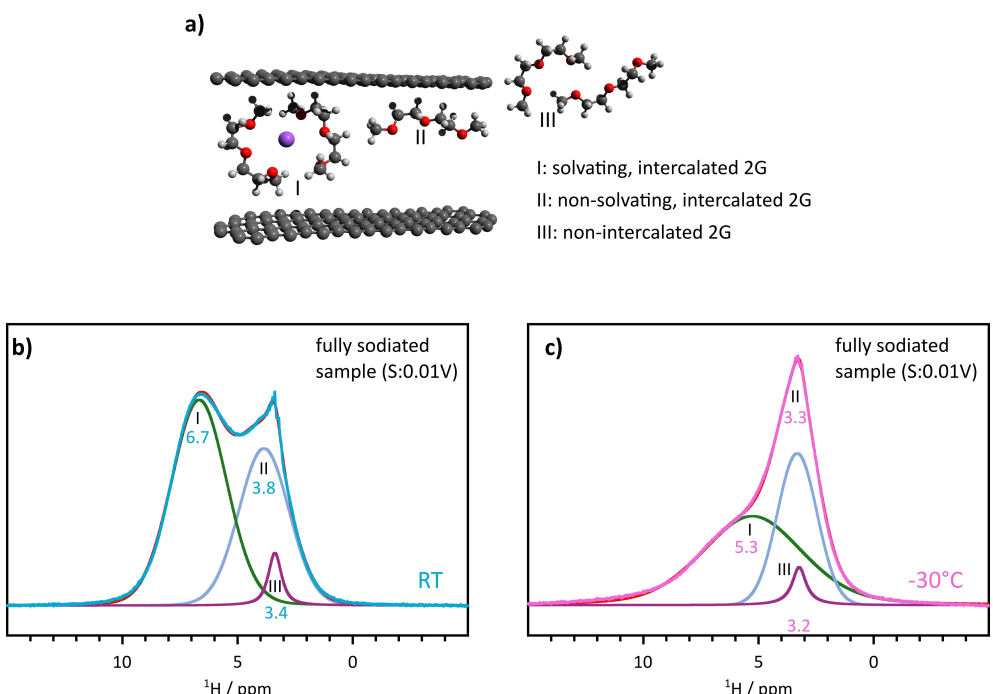


Figure 2. a) Schematic representation of the different proton species, b and c) ^1H single pulse MAS NMR spectra from fully intercalated sodium ions in graphite using 1 M NaOTf in diglyme as electrolyte b) at room temperature (RT) and c) -30°C .

^2H NMR of chemically intercalated sodium ions, showing more rigidly bond 2G to the sodium ion at -40°C compared to RT.^[18] Investigation of lithium ions co-intercalated in graphite (see Supporting Information Figures S2 and S3) also revealed two different signals. A further discussion on this is given in the Supporting Information.

As already proven with ^{13}C NMR, variations can be seen between different SOCs. To get further insights, *ex situ* ^1H single pulse NMR experiments were conducted at different voltages (see Figure 3). The already discussed, fully co-intercalated sample is represented by S:0.01V in this Figure. Comparing the evolution of type I 2G molecules (2G surrounding sodium ions in the graphitic lattice) one can see that the line broadening is strongly changing before/during and after the voltage plateau (comparison of S:0.45 and S:0.01V versus S:1V, S:0.625V and D:0.7V). The reader is referred to the Supporting Information Table S2 for the Full Width at Half Maximum (FWHM) values and intensity ratios obtained by the signal deconvolutions. The line broadening is significantly larger for voltages above or at the plateau, indicating a reduced mobility of glyme molecules coordinated to sodium ions in the graphitic lattice at low degrees of sodiation. This might be explained by a lower interlayer distance where the amount of intercalated material is low. At S:0.45 and S:0.01V, where the graphite is (almost) completely sodiated, the mobility of the $[\text{Na}(2\text{G})_y]^+$ complexes increases again in agreement with a large interlayer distance in this case. Also, even though a large amount ($\sim 77\%$ discharge capacity for S:0.45 and $\sim 97\%$ for S:0.01V, compared to the first discharge capacity) of $[\text{Na}(2\text{G})_y]^+$ complexes is intercalated, they do not significantly hinder each other's movement.

Regarding the similarity of S:0.45V and S:0.01V the reader is referred to the Supporting Information (Figure S4).

A similar effect can be seen for the non-solvating intercalated 2G molecules in the graphite (see Supporting Information Table S2 for the FWHM values and intensity ratios), showing a reduced mobility at lower states of sodiation which might be explained also by a lower interlayer distance. Unlike to the broadening that was visible at -30°C , that only took place for the bulky $[\text{Na}(2\text{G})_y]^+$ complex (type I), also the non-solvating 2G molecules show an increased line broadening at low states of sodiation even at RT, showing that the mobility of all types of glymes is affected by the SOC. This effect is reversible, as a broadening of the peaks can be seen during the deintercalation process (D:0.7V).

In addition, sharp peaks, indicating excess 2G can be seen in almost every sample, indicating that the samples are not dried out. A difference in the intensity results from the fact that *ex situ* experiments were performed and different samples/cells have been used for the different SOCs. This also explains the differences between S:2V and D:2V as more free electrolyte might be attached to the D:2V. The broad peak visible at D:2V might be related to irreversible trapped or adsorbed 2G molecules.

The ^{23}Na NMR spectra of fully intercalated graphite (S:01V) is shown in Figure 4a). At least two signals are expected in this case for sodium sites at residual free electrolyte outside of the graphite structure and sodium ions co-intercalated in graphite. The overlap of the signals observed complicates the assignment of the spectrum. The peak width for the electrolyte site was constrained to not go above 200 Hz during fitting. The peak width of the pure electrolyte was measured to be 113 Hz

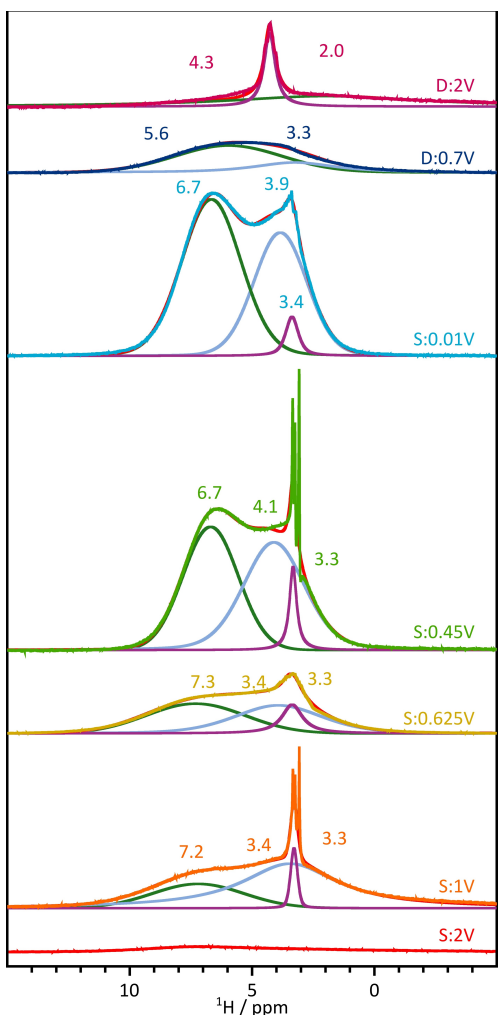


Figure 3. ^1H single pulse MAS NMR spectra of co-intercalated sodium ions in graphite stopped at different states of charge, the voltage profile is displayed in Figure 1.

(see Figure S5), which should be similar for the *ex situ* samples. Therefore, two sites could be fit with reasonable accuracy. The peak at -6.3 ppm is in agreement with the shift obtained for the NaOTf electrolyte in 2G. (comparison spectra for 1 M NaOTf in different glymes can be found in Figure S5). The mean peak at -4.6 ppm is assigned to sodium ions inside of the graphene layers. The increased signal width of the intercalated sodium ions as compared to the free electrolyte can be explained by a decrease in mobility of the first. The lack of an extensive down-field shift indicates that the sodium ions are solvated and do not experience a strong Knight-shift character as it is the case for lithium intercalation in graphite, where larger shifts are characteristic for an increase in metallicity of lithium.^[19] In the case of lithium, three peaks are visible. A more detailed explanation and the corresponding graphs can be found in the Supporting Information (Figure S 3b).

Figure 4c) shows the ^{23}Na NMR spectra at the same points of (de)sodiation as for the *ex situ* ^{13}C (Figure 1b) and ^1H NMR experiments (Figure 3). It clearly indicates that both types of sodium ions exist in all (partially) sodiated samples. It is noted

here, that it is difficult to distinguish between sodium ions solvated by one or two 2Gs in ^{23}Na NMR as it is expected for these signals to be in a similar shift range. Thus, it cannot be concluded that the peak at around -4.6 ppm corresponds to one sodium site only. Instead, a combination of co-intercalated sodium sites with different 2G solvation environments is more likely, possibly changing with the state of sodiation. Interestingly, S:0.45V and S:0.01V differ from S:1V, S:0.625V and D:0.7V in intensity, peak width and peak shift. A higher intensity, peak width and an increased shift value can be seen at S:0.45V and S:0.01V, indicating a phase transition at high co-intercalation levels. Distinct differences between the S:0.45V and S:0.01V compared to the other samples can be also seen in the ^1H and ^{13}C NMR experiments.

The residual small peaks at fully de-intercalated state after the 1st cycle (S:2V) and the 2nd cycle (D:2V) can be assigned to irreversibly trapped or adsorbed sodium ions or free electrolyte. However, it has to be mentioned that the ICE is high (91%–97%) which suggests that trapping of ions can be (if at all) only a minor effect. Note that for the used electrolyte composition, there is also hardly any evidence for a solid electrolyte interphase.^[6,20]

Information on 2G dynamics in sodium t-GICs

To further elucidate the storage mechanism and get information about the 2G dynamics within the graphitic lattice, exchange experiments of proton magnetization (2D ^1H - ^1H EXSY NMR) were performed for the sample S:0.01V. Clear off-diagonal signals are observed in such an experiment recorded with a mixing time of 0.1 s. The presence of off-diagonal signals in this experiment can be ascribed to a magnetization transfer effect between distinct proton positions under the effect of nuclear dipolar couplings, or by the physical exchange between both environments during the mixing time of the experiment. If the exchange signals are induced by physical exchange of atoms or molecules, their rate is expected to decrease at lower temperatures as this is a mechanism determined by an activation energy. On the contrary, the observed exchange rates shown in Figure 5b) reveal faster exchange rates at lower temperatures (0°C). This agrees with an homonuclear spin diffusion mechanism, as dipolar interactions are generally stronger at lower temperatures where dynamics are reduced. This result shows that the sodium ions diffuse together with 2G molecules rather than hop between different molecules (within the time frame of the experiment, here 0.1 s). A schematic representation of the mechanism is shown in Figure 5c). To the best of our knowledge this mechanism was not reported before and gives new insights into the storage mechanism and mobility of sodium ions co-intercalated in a graphitic lattice.

Comparison between 2G, 3G and 5G as an electrolyte solvent

Apart from 2G, also other solvents in the series of linear glymes can be used to co-intercalate sodium ions in graphite and have

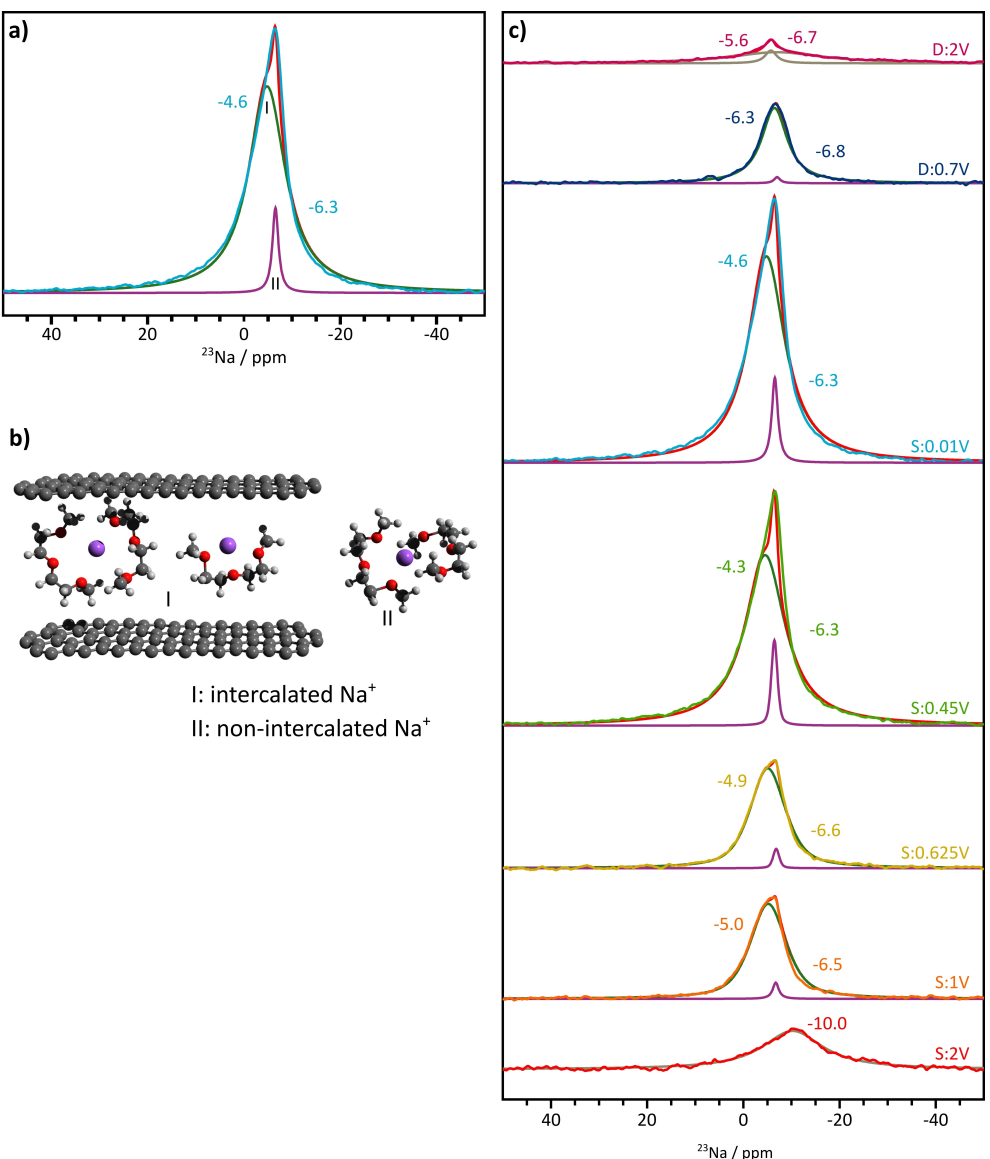


Figure 4. a) ^{23}Na MAS NMR spectrum from fully intercalated sodium ions in graphite using 1 M NaOTf in diglyme as electrolyte. b) Schematic representation of the different sodium species. c) ^{23}Na MAS NMR spectra of co-intercalated sodium ions in graphite stopped at different states of charge, the voltage profile is displayed in Figure 1.

been studied by various methods.^[3b,5,6d,e,j] However, a systematic study by ss-NMR on the effect of different glymes is lacking so far. 3G and 5G have opposing properties in the series of glymes, as they are proposed to have the most unfavorable coordination (3G) as well as a favorable coordination (5G). In the case of 5G, the number of oxygen atoms is the same compared to two 2G molecules and 2G is known to show a good cycling performance.^[3b,5,6i-m,21] Electrochemical cycling for 3G and 5G has been performed at elevated temperatures (60 °C) as otherwise no sufficient cycling is possible, which might result from a bad solvation in the case of 3G and a high viscosity of the 5G.^[6e] The corresponding cycling curves can be found in the Supporting Information in Figure S6. 5G shows a similar discharge capacity and voltage profile compared to 2G with an additional small plateau at 0.12 V. In contrast, the voltage profile of the 3G cell does not show a clear plateau at

all and just exhibits capacities of around 80 mAh g⁻¹ (around 100 mAh g⁻¹ are obtained for 2G and 5G). It was found that the reaction is kinetically, not thermodynamically controlled, and its poor behavior might originate from an unfavorable coordination.^[6e]

Similar to the results from 2G, different proton species can be seen in the ^1H NMR spectra recorded for the *ex situ* samples of fully co-intercalated glymes (see Figure 6a). This can be correlated to the solvent molecules solvating sodium ions (type I) and non-solvating electrolyte molecules (type II) in the graphite. The third species, non-solvating electrolyte out of the graphite, is not visible for every electrolyte, which might be because cells with 3G and 5G had to be cycled at elevated temperature. Interestingly, the peaks for both type I and II in the 3G sample are about 1.6 times broader than in the 2G case (5G 1.1 times broader than 2G) indicating a slower intrinsic

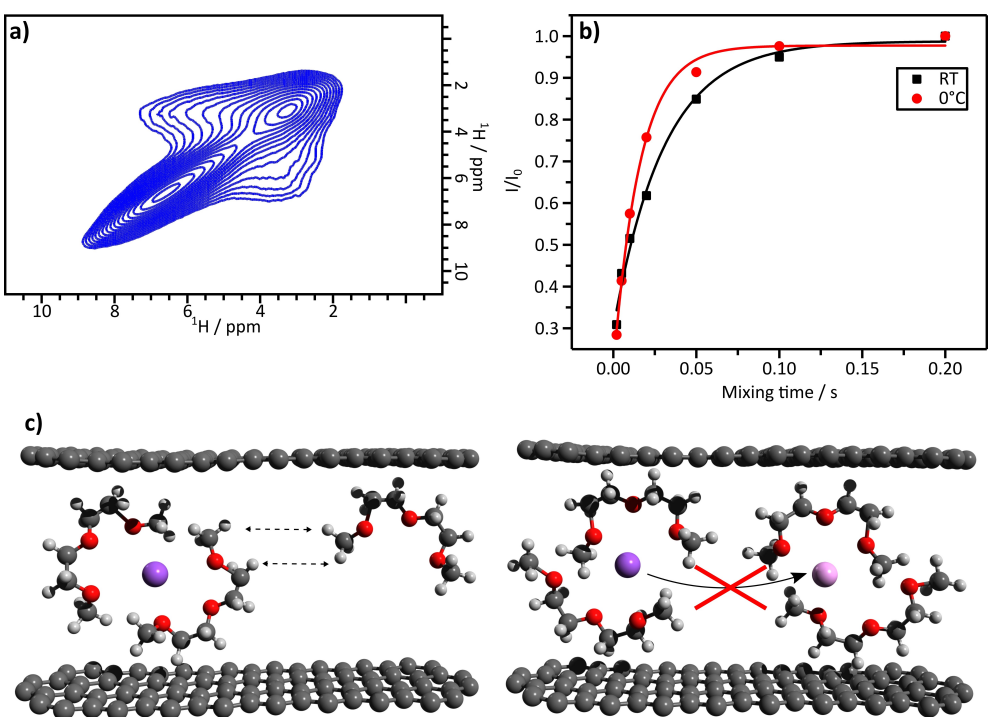


Figure 5. a) Exchange NMR experiments of proton magnetization (EXSY) of fully intercalated sodium ions in graphite using 1 M NaOTf in diglyme as electrolyte at 0°C and 0.1 s mixing time. b) Relative intensity related to the mixing time for the EXSY experiment at room temperature (RT) and 0°C . c) Schematic illustration of the mechanism gained through the EXSY experiments.

mobility of the intercalated 3G molecules as compared to 2G and 5G. This cannot be correlated to the viscosity of the solvent, as it is the highest for 5G.^[6e] In contrast, it can be ascribed to a sterically hindered movement of the $[\text{Na}(3\text{G})_y]^+$ complex in the graphitic lattice, which could be explained by either an under- or overcoordination of the sodium ion with one or two 3G molecules, respectively.^[3b,6d]

${}^{23}\text{Na}$ single pulse experiments at RT are presented, next to others, in Figure 6b) and further analyzed (line deconvolution) in Figure S7, proving that sodium ions with two different local environments are present in the 3G and 5G samples as well. They can be assigned to sodium ions co-intercalated into the graphitic structure (type I see Figure 4) and sodium ions at free electrolyte not experiencing the local environment of graphite (type II), and therefore existing outside of the graphitic structure. A high ratio between intercalated and non-intercalated sodium ions for all different glymes indicate the successful co-intercalation of sodium ions with all glymes. It has to be mentioned that a quantitative comparison between the different glymes is not possible in this case. Therefore, no conclusions can be drawn between the discharge capacity (amount of intercalated sodium ions) and the peak area. The peak shifts vary slightly depending on the electrolyte used, a similar phenomenon has been also observed in liquid NMR of the pure electrolytes (see Supporting Information Figure S5) and can be assigned to the different solvent effects in the electrolyte.^[22]

${}^1\text{H}-{}^{23}\text{Na}$ cross polarization (CP) NMR experiments have been performed to study the interaction between the glymes and

the coordinated sodium ions. The CP experiments obtained at different temperatures as well as the corresponding single pulse experiments are plotted in Figure 6b). No signals were observed for ${}^1\text{H}-{}^{23}\text{Na}$ CP spectra of 2G and 5G at RT. The lack of CP magnetization transfer is ascribed to the presence of rapid local oscillations that effectively average out heteronuclear interactions. We therefore conclude that rapid movements of 2G and 5G molecules around sodium ions exist at RT. Reducing the temperature to -30°C is necessary to stop these motions resulting in the observation of a CP signal at around -9 ppm (2G) and two signals at -7 ppm and -13 ppm (5G). Gotoh et al. exhibited a similar mobility behavior for chemically synthesized *t*-GICs with 2G as electrolyte solvent, showing a high mobility of the 2G molecule around the sodium ion at RT, with the central oxygen atom of the 2G weakly coordinated to the sodium ion. At low temperatures (below -40°C) the 2G molecules are coordinated rigidly to the sodium ion.^[18] A splitting up from one signal at around -9 ppm at RT to two at -7 ppm and -12 ppm at -30°C for 5G is also visible in the single pulse ${}^{23}\text{Na}$. This peak split can be possibly explained by the fact that dynamic processes are hindered at low temperatures and therefore results in a better visibility of two distinct sodium sites. For 3G the transfer of magnetization is already visible at RT indicated by a CP signal at -10 ppm . This can be referred to a hindered motion of the 3G molecule around the sodium ions, probably due to an unfavorable coordination or a reduced interlayer distance. A similar phenomenon, with visible interactions already at RT, is also apparent for co-intercalated

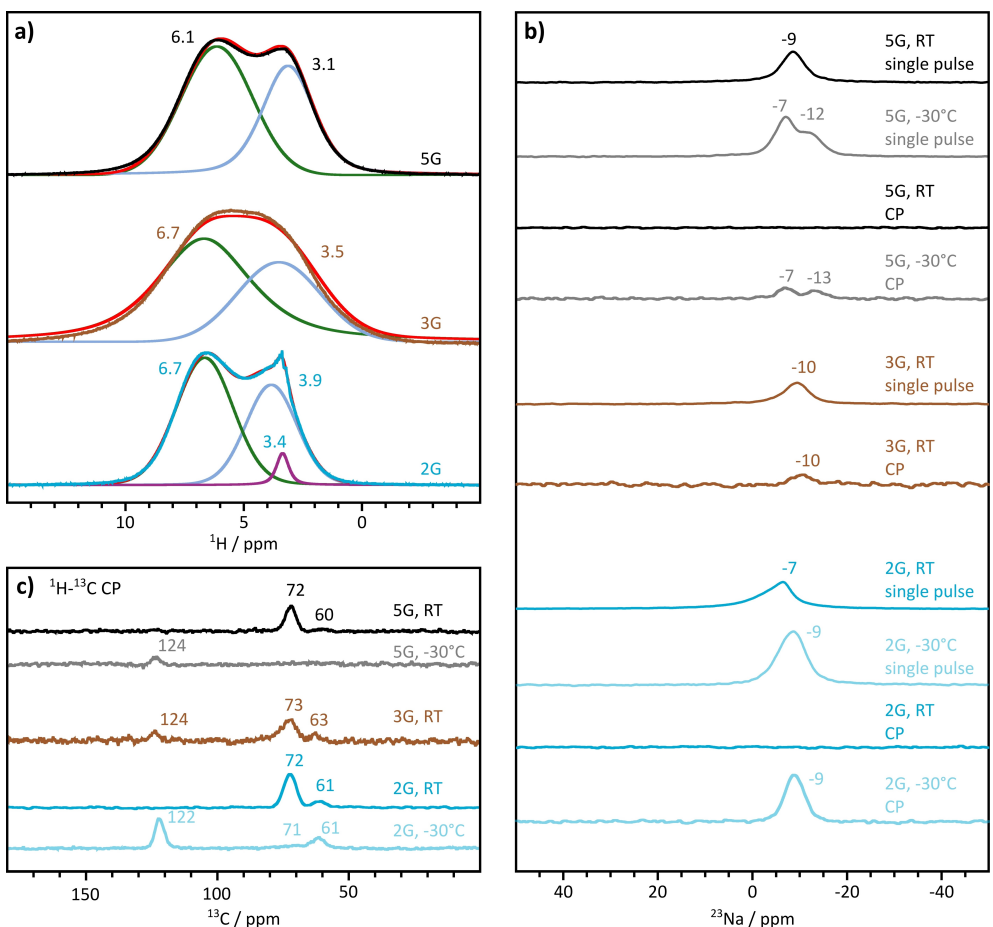


Figure 6. Investigation of fully intercalated sodium ions in graphite using 1 M NaOTf in diglyme (2G), triglyme (3G) and pentaglyme (5G) as electrolyte. a) ¹H single pulse spectra, b) ¹H-¹³C cross polarization (CP) spectra (RT and -30 °C), c) ²³Na single pulse as well as ¹H-²³Na CP spectra (RT and -30 °C).

lithium ions (see Supporting Information Figure S3c), which might result from a smaller ion size of the lithium ion.^[1a]

In addition, ¹H-¹³C CP experiments have been performed to gain information about the dipole-dipole interactions between solvent protons and carbons at the graphite for the different glymes (see Figure 6c). Peaks at ~72 ppm and ~61 ppm can be correlated to the methylene group (CH_2) and methyl (CH_3) group in the glyme molecule, respectively. They are visible for all different glymes at RT, however showing various line broadenings due to differing viscosities of the glyme molecules^[6e] and therefore different mobilities. At -30 °C they exhibit an additional broadening, the extent of which depends on the type of glyme. For 5G, no peaks are visible anymore as the movement of the larger 5G molecule is so slow, that the signal disappears in the baseline due to severe line broadening.

The presence of a ¹³C CP signal in Figure 6c) at around 122–124 ppm indicates a ¹H to ¹³C heteronuclear dipolar interaction of the glyme molecules (the only source of protons in the sample) with the ¹³C isotopes of the graphitic lattice. Such correlation is not visible for 2G and 5G at RT, proving a high mobility of those molecules in the graphitic lattice. The result for 2G is in line with the outcomes from Leifer et al., indicating a high mobility of the $[\text{Na}(2\text{G})]^{+}$ complex at RT.^[8] However, reducing the temperature to -30 °C a ¹H-¹³C CP signal is

observed, that proves a restricted mobility at such low temperatures. 5G shows a similar behavior as it has the same number of oxygens compared to two 2G molecules. Therefore, a similar interaction/dynamic behavior between graphite and the glymes is expected. In contrast to 2G and 5G, an interaction between graphite and 3G (signal at 124 ppm) can already be seen at RT (similar as for the co-intercalation of lithium ions see Figure S3d). This clearly shows that the mobility of the $[\text{Na}(3\text{G})]^{+}$ complex inside the graphitic lattice is already limited at RT, in agreement with the ¹H NMR results. Slower diffusion rates for the $[\text{Na}(3\text{G})]^{+}$ complex compared to a $[\text{Na}(4\text{G})]^{+}$ complex were also found by Seidl et al.^[6d] A lower mobility of the $[\text{Na}(3\text{G})]^{+}$ complex might be explained by an unfavorable coordination of the sodium ion (either over- or under-coordination).

Conclusion

ss-NMR has been used to study the local interactions of sodium ions in *t*-GICs with 2G as the electrolyte solvent at different SOCs. ¹³C NMR measurements revealed that the solvation structure and local interactions between the graphene layers and the sodium ions change depending on the SOC. At low

levels of sodiation it appears that a co-existence of one and two 2G molecules per sodium ion is visible, whereas at high levels of sodiation the coordination of two 2G molecules is favored. However, other factors might also influence the shift of the ^{13}C NMR signal. Solvating as well as non-solvating 2G molecules between the graphene layers have been found using ^1H NMR. In addition, 2G and the $[\text{Na}(2\text{G})_2]^+$ complex are more mobile at higher levels of sodiation. ^{23}Na experiments confirm the phase change at the plateau region, measured already by other techniques. 2D ^1H - ^1H EXSY experiment helped to get a further understanding of the transport mechanism. As an important finding, intercalated sodium ions stick to their 2G molecule(s) and do not hop between different molecules. In addition, 3G and 5G have been also used as electrolyte solvent and differences in the mobility have been found for those. ^1H as well as cross polarization experiments revealed that 3G as well as the $[\text{Na}(3\text{G})_2]^+$ complex have a reduced mobility compared to 2G and 5G. In addition, for 3G an increased interaction between the graphene layers and the solvent molecules as well as the sodium ions and the solvent molecules is visible already at RT. In contrast, those interaction only appear at -30°C for 2G and 5G. Overall, the use of 2G leads to t-GICs with the highest mobility of the intercalated species. This means this solvent is most favorable in case of high-rate applications.

Experimental Section

Electrochemical measurements for ss-NMR

Electrochemical measurements for ss-NMR were conducted in a 2-electrode set-up (CR2032 coin cells by MTI Corp.) with the pure graphite (MTI Corp.) as working electrode and sodium (BASF) or lithium (Rockwood Lithium) as counter electrode. Pure graphite powder was used to avoid influences from a binder material on the ss-NMR results. Galvanostatic charge and discharge experiments with potential limitation (GCPL) experiments were performed with a rate of 0.1 C (11 mA/g) in a voltage range of 0.01–2 V vs. Na^+/Na and 0.1–2 V vs. Li^+/Li . The lower cut-off potential was limited to 0.1 V in the case of lithium to avoid the formation of an additional plateau slightly below 0.1 V, which might result from the formation of binary graphite intercalation compounds. Measurements with 2G were conducted at RT, experiments with 3G and 5G were conducted in an oven (Binder KB 53) at 60°C . A BCS 805 was used as battery cycler. One initial cycle was performed before the cells were stopped at the specific voltage in the second cycle. Unless otherwise specified the cells were opened in an argon-filled glovebox (MBraun), the graphite powder was removed and packed tightly until the ss-NMR measurements were performed to avoid evaporation of the solvent. For further information on the experiments on drying the reader is referred to the Supporting Information.

Electrolyte

1 M NaOTf (purity > 98.0%, TCI) in diethylene glycol dimethyl ether (diglyme, 2G), triethylene glycol dimethyl ether (triglyme, 3G) (both purchased from Sigma-Aldrich), and pentaethylene glycol dimethyl ether (pentaglyme, 5G) (Nippon Nyukazai Co., Ltd.) and 1 M LiOTf

(99.995 % trace metal basis, Sigma-Aldrich) in 2G have been used as electrolyte.

ss-NMR experiments

If not otherwise specified, Magic Angle Spinning Nuclear Magnetic Resonance (MAS NMR) experiments were performed using a Bruker Avance III 500 spectrometer equipped with a standard 2.5 mm probe. Spectra were recorded at an MAS frequency of 10 kHz. ^{23}Na , ^7Li spectra were referenced to 0.1 M LiCl and 0.1 M NaCl solutions. ^{13}C and ^1H spectra were referenced indirectly to a solid adamantane sample resonating at 38.48 ppm and ^1H bulk water resonating at 4.8 ppm. ^{13}C experiments were recorded using a Hahn Echo experiment with a 90° pulse of 2.5 μs and a recycle delay of 15 s with 3649 to 15890 scans. ^1H experiments shown in Figures 2 and 3 (Na/2G) were recorded using single 90° pulses of 4.7 μs and a recycle delay of 3 s. For ^1H experiments shown in Figure 6 and Figure S3 (Na/3G, Na/5G and Li/2G) the pulse length was 1.9 μs and the recycle delay 5 s. ^{23}Na 1D experiments were obtained accumulating 52 to 800 scans and single 1.3 to 1.5 μs pulses with a recycle delay of 3 to 5 s. ^7Li 1D experiments were obtained accumulating 16 scans and single 2.4 μs pulses with a relaxation delay of 20 s. The ^1H - ^{13}C CP spectra were obtained using 1.0 to 2.0 ms mixing time, a 2.5 μs ^1H pulse and 3 to 5 s recycle delays with 1215 to 46297 scans. The ^1H - ^{23}Na CP spectra were obtained using 2 ms mixing time, a 2.5 μs ^1H pulse and 3 to 4 s recycle delays with 200 to 16720 scans. The ^1H - ^7Li CP spectrum was obtained using a 1 ms mixing time, a 2.5 μs ^1H pulse and 3 s recycle delay with 64 scans. EXSY (2D EXchange SpectroscopY) experiments were performed using a standard three-pulse sequence with mixing times specified in each experiment.

For the investigations of the drying phenomena, shown in the Supporting Information (Figure S1), ^{13}C MAS NMR experiments were performed at 9.4 T using a Bruker 400DNP Ascend spectrometer equipped with a 4.0 mm probe. Spectra were recorded at an MAS frequency of 10 kHz. Spectra were referenced to a solid adamantane sample resonating at 38.48 ppm. ^{13}C Hahn-echo experiments were obtained using 90° pulses of 5.0 μs with a recycle delay of 15 s and 4715 to 4869 scans. Samples were diluted with either MgO powder or glass fiber separator to enable sample spinning.

Liquid ^{23}Na NMR spectra were performed at 9.4 T using a Bruker 400DNP Ascend spectrometer equipped with a 5 mm broadband probe. 1 M NaCl was used as a standard solution for ^{23}Na (0 ppm). Experiments were obtained using 90° pulses of 71 μs with a recycle delay of 4 s and 64 scans.

Spectra were plotted and deconvoluted using the TopSpin and the Dmfit^[23] software.

Acknowledgements

This project has received funding from the European Research Council (ERC) under the European Union's Horizon 2020 research and innovation program (grant agreement no. [864698]), and from the EIG Concert Japan program (LIBRA, BMBF 01DR18003). The authors thank BASF for providing high-purity sodium. Open Access funding enabled and organized by Projekt DEAL.

Conflict of Interest

The authors declare no conflict of interest.

Data Availability Statement

The data that support the findings of this study are available from the corresponding author upon reasonable request.

Keywords: co-intercalation • electrochemistry • graphite • sodium-ion battery • solid-state NMR spectroscopy

- [1] a) P. Adelhelm, P. Hartmann, C. L. Bender, M. Busche, C. Eufinger, J. Janek, *Beilstein J. Nanotechnol.* **2015**, *6*, 1016–1055; b) J. Asenbauer, T. Eisenmann, M. Kuenzel, A. Kazzazi, Z. Chen, D. Bresser, *Sustain. Energy Fuels* **2020**, *4*, 5387–5416; c) C. Mao, M. Wood, L. David, S. J. An, Y. Sheng, Z. Du, H. M. Meyer III, R. E. Ruther, D. L. Wood III, *J. Electrochem. Soc.* **2018**, *165*, A1837.
- [2] a) P. K. Nayak, L. Yang, W. Brehm, P. Adelhelm, *Angew. Chem. Int. Ed.* **2018**, *57*, 102–120; *Angew. Chem.* **2018**, *130*, 106–126; b) J.-Y. Hwang, S.-T. Myung, Y.-K. Sun, *Chem. Soc. Rev.* **2017**, *46*, 3529–3614; c) Y. Fang, L. Xiao, Z. Chen, X. Ai, Y. Cao, H. Yang, *Electrochim. Energy Rev.* **2018**, *1*, 294–323; d) N. Tapia-Ruiz, A. R. Armstrong, H. Alptekin, M. A. Amores, H. Au, J. Barker, R. Boston, W. R. Brant, J. M. Brittain, Y. Chen, M. Chhowalla, Y.-S. Choi, S. I. R. Costa, M. Crespo Ribadeneyra, S. A. Cussen, E. J. Cussen, W. I. F. David, A. V. Desai, S. A. M. Dickson, E. I. Eweka, J. D. Forero-Sabaya, C. P. Grey, J. M. Griffin, P. Gross, X. Hua, J. T. S. Irvine, P. Johansson, M. O. Jones, M. Karlsmo, K. E. E. Kim, O. V. Kolosov, Z. Li, S. F. L. Mertens, R. Mogensen, L. Monconduit, R. E. Morris, A. J. Naylor, S. Nikman, C. A. O'Keefe, D. M. C. Ould, R. G. Palgrave, P. Poizot, A. Ponrouch, S. Renault, E. M. Reynolds, A. Rudola, R. Sayers, D. O. Scanlon, S. Sen, V. R. Seymour, B. Silván, M. T. Sougrati, L. Stievano, G. S. Stone, C. I. Thomas, M.-M. Titirici, J. Tong, T. J. Wood, D. S. Wright, R. Younesi, *J. Phys. Energy* **2021**, *3*, 031503.
- [3] a) B. Jache, P. Adelhelm, *Angew. Chem. Int. Ed.* **2014**, *53*, 10169–10173; *Angew. Chem.* **2014**, *126*, 10333–10337; b) B. Jache, J. O. Binder, T. Abe, P. Adelhelm, *Phys. Chem. Chem. Phys.* **2016**, *18*, 14299–14316.
- [4] a) Y. Liu, B. V. Merinov, W. A. Goddard III, *Proc. Nat. Acad. Sci.* **2016**, *113*, 3735–3739; b) H. Moriwake, A. Kuwabara, C. A. J. Fisher, Y. Ikuhara, *RSC Adv.* **2017**, *7*, 36550–36554; c) O. Lenchuk, P. Adelhelm, D. Mollenhauer, *Phys. Chem. Chem. Phys.* **2019**, *21*, 19378–19390.
- [5] H. Kim, J. Hong, Y.-U. Park, J. Kim, I. Hwang, K. Kang, *Adv. Funct. Mater.* **2015**, *25*, 534–541.
- [6] a) H. Kim, J. Hong, G. Yoon, H. Kim, K.-Y. Park, M.-S. Park, W.-S. Yoon, K. Kang, *Energy Environ. Sci.* **2015**, *8*, 2963–2969; b) A. P. Cohn, K. Share, R. Carter, L. Oakes, C. L. Pint, *Nano Lett.* **2016**, *16*, 543–548; c) H. Kim, G. Yoon, K. Lim, K. Kang, *Chem. Commun.* **2016**, *52*, 12618–12621; d) L. Seidl, N. Bucher, E. Chu, S. Hartung, S. Martens, O. Schneider, U. Stimming, *Energy Environ. Sci.* **2017**, *10*, 1631–1642; e) M. Goktas, B. Akduman, P. Huang, A. Balducci, P. Adelhelm, *J. Phys. Chem. C* **2018**, *122*, 26816–26824; f) M. Goktas, C. Bolli, E. J. Berg, P. Novák, K. Pollok, F. Langenhorst, M. v. Roeder, O. Lenchuk, D. Mollenhauer, P. Adelhelm, *Adv. Energy Mater.* **2018**, *8*, 1702724; g) J. Rodríguez-García, I. Cameán, A. Ramos, E. Rodríguez, A. B. García, *Electrochim. Acta* **2018**, *270*, 236–244; h) H. Zhang, Z. Li, W. Xu, Y. Chen, X. Ji, M. M. Lerner, *Nanotechnology* **2018**, *29*, 325402; i) M. Goktas, C. Bolli, J. Buchheim, E. J. Berg, P. Novák, F. Bonilla, T. Rojo, S. Komaba, K. Kubota, P. Adelhelm, *ACS Appl. Mater. Interfaces* **2019**, *11*, 32844–32855; j) N. Karimi, A. Varzi, S. Passerini, *Electrochim. Acta* **2019**, *304*, 474–486; k) Z.-L. Xu, G. Yoon, K.-Y. Park, H. Park, O. Tamwattana, S. J. Kim, W. M. Seong, K. Kang, *Nat. Commun.* **2019**, *10*, 2598; l) Z. Wang, H. Yang, Y. Liu, Y. Bai, G. Chen, Y. Li, X. Wang, H. Xu, C. Wu, J. Lu, *Small* **2020**, *16*, 2003268; m) I. Escher, Y. Kravets, G. A. Ferrero, M. Goktas, P. Adelhelm, *Energy Technol.* **2021**, *9*, 2000880.
- [7] Z. Zhu, F. Cheng, Z. Hu, Z. Niu, J. Chen, *J. Power Sources* **2015**, *293*, 626–634.
- [8] N. Leifer, M. F. Greenstein, A. Mor, D. Aurbach, G. Goobes, *J. Phys. Chem. C* **2018**, *122*, 21172–21184.
- [9] G. Yoon, H. Kim, I. Park, K. Kang, *Adv. Energy Mater.* **2017**, *7*, 1601519.
- [10] S. C. Jung, Y.-J. Kang, Y.-K. Han, *Nano Energy* **2017**, *34*, 456–462.
- [11] A. C. S. Jensen, H. Au, S. Gärtnner, M. M. Titirici, A. J. Drew, *Batteries & Supercaps* **2020**, *3*, 1306–1310.
- [12] Q. Wei, X. Chang, J. Wang, T. Huang, X. Huang, J. Yu, H. Zheng, J. h. Chen, D. L. Peng, *Adv. Mater.* **2022**, *34*, 2108304.
- [13] T. J. Bruno, P. D. N. Svoronos, *CRC Handbook of Chemistry and Physics*, 95. ed., Taylor and Francis Group, Boca Raton, **2014**.
- [14] C.-J. Yu, S.-B. Ri, S.-H. Choe, G.-C. Ri, Y.-H. Kye, S.-C. Kim, *Electrochim. Acta* **2017**, *253*, 589–598.
- [15] H.-J. Liang, B.-H. Hou, W.-H. Li, Q.-L. Ning, X. Yang, Z.-Y. Gu, X.-J. Nie, G. Wang, X.-L. Wu, *Energy Environ. Sci.* **2019**, *12*, 3575–3584.
- [16] Y. Okamoto, *J. Phys. Chem. C* **2014**, *118*, 16–19.
- [17] Z. Chen, C. S. Wannere, C. Corminboeuf, R. Puchta, P. v. R. Schleyer, *Chem. Rev.* **2005**, *105*, 3842–3888.
- [18] K. Gotoh, H. Maruyama, T. Miyatou, M. Mizuno, K. Uruta, H. Ishida, *J. Phys. Chem. C* **2016**, *120*, 28152–28156.
- [19] A. I. Freytag, A. D. Pauric, S. A. Krachkovskiy, G. R. Goward, *J. Am. Chem. Soc.* **2019**, *141*, 13758–13761.
- [20] X.-r. Zhang, J.-y. Yang, Z.-y. Ren, K.-y. Xie, Q. Ye, F. Xu, X.-r. Liu, *New Carbon. Mater.* **2022**, *37*, 371–379.
- [21] a) P. Han, X. Han, J. Yao, L. Zhang, X. Cao, C. Huang, G. Cui, *J. Power Sources* **2015**, *297*, 457–463; b) R. Klee, M. Wiatrowski, M. J. Aragón, P. Lavela, G. F. Ortiz, R. Alcántara, J. L. Tirado, *ACS Appl. Mater. Interfaces* **2017**, *9*, 1471–1478; c) T. Kajita, T. Itoh, *Phys. Chem. Chem. Phys.* **2018**, *20*, 2188–2195.
- [22] L. Lutz, W. Yin, A. Grimaud, D. Alves Dalla Corte, M. Tang, L. Johnson, E. Azaceta, V. Sarou-Kanian, A. J. Naylor, S. Hamad, J. A. Anta, E. Salager, R. Tena-Zaera, P. G. Bruce, J.-M. Tarascon, *J. Phys. Chem. C* **2016**, *120*, 20068–20076.
- [23] D. Massiot, F. Fayon, M. Capron, I. King, S. Le Calvé, B. Alonso, J. O. Durand, B. Bujoli, Z. Gan, G. Hoatson, *Magn. Reson. Chem.* **2002**, *40*, 70–76.

Manuscript received: September 23, 2022

Revised manuscript received: November 8, 2022

Accepted manuscript online: November 15, 2022

Version of record online: January 3, 2023